Calculation of the *P-T* phase diagram of Zr in different approximations for the exchange-correlation energy

S. A. Ostanin and V. Yu. Trubitsin
Physico-Technical Institute, Ural Branch of Russian Academy of Sciences, 132 Kirov Street, 426001 Izhevsk, Russia
(Received 27 August 1997)

The full-potential linear muffin-tin orbital method is used within the local density approximation and generalized gradient approximation (GGA) to calculate the total energy and equilibrium lattice properties for the observed phases of Zr. The temperature dependences of the free energy, specific volume, bulk modulus, Debye temperature, and Grüneisen constant are found for these structures within the Debye model. For most quantities, a good quantitative agreement with experiment is obtained. The *P-T* phase diagram constructed from the calculated thermodynamical Gibbs potentials within the GGA fits well the available room-temperature data on the $\alpha \rightarrow \omega$ and $\omega \rightarrow \beta$ transitions. At ambient pressure, we get $T_{\beta \rightarrow \alpha} = 1193$ K, which is close to the observed value. [S0163-1829(98)02514-4]

INTRODUCTION

The central problem of the microscopic description of structural transformations occurring in metals under pressure consists in introducing a consistent model for finite temperatures.[1] The simplest way to investigate the structural phase transitions on the basis of first-principles binding curves is to use the Debye-Grüneisen theory. There are two approaches in using the Debye model for the study of the lattice properties based on *ab initio* calculations. In the first approach, the pair potential is constructed in terms of cohesive energy,[2] then the dynamical matrix is calculated, and the Debye temperature Θ_D is determined through the mean frequency of the vibrational spectrum. The results obtained in such a way[3] are not always satisfactory, and the temperature dependences of lattice properties are difficult to calculate.

In the second approach, after having performed the total energy calculation, the characteristic Debye temperature Θ_D is calculated in terms of the bulk modulus B, and then the free energy $F(T,V)$ is found as a function of Θ_D and the volume V. The applicability of this method to the study of particular metals is restricted by the isotropic Debye model and the assumption of the mean sound velocity v. Earlier, using the averaging of the mean sound velocity for cubic metals,[4] the authors of Ref. 5 calculated the temperature properties of 14 bcc and fcc metals within the Debye model. The temperature dependence of the lattice constant and the linear thermal expansion coefficient calculated by minimizing the free energy with respect to the volume agree quite well with the experimental data. Thus the method mentioned seems to be appropriate for cubic metals. Similar investigations for transition metals, in which the ground state has a noncubic lattice and the cubic-type structures are high-pressure and high-temperature phases, were not performed.

The systems considered at high temperatures and high pressures require the allowance for anharmonic effects which are very essential in these regions. The Debye form of the harmonic approximation is rather crude theory. Recently, we suggested a model of instability evolution for the martensitic transformation in bcc Zr (Ref. 6) which takes into account the anharmonicity effects within the framework of a pseudoharmonic self-consistent phonon approximation.[7] In the present work we calculate from first principles the *P-T* phase diagram of Zr in the Debye model and demonstrate that this simplified approach is quite sufficient for the problem under consideration. Earlier, we carried out an analogous investigation of the Ti interfaces which gave a good agreement with experiments.[8] The Zr interfaces, in the case of simultaneously high temperature and pressure, are not clearly defined as yet. At ambient pressure, with temperature elevation Zr undergoes the transformation from a stable room-temperature hcp structure (α phase) into the bcc one (β phase). The latter persists up to the melting temperature. The temperature $T^{\alpha \rightarrow \beta} = 1136$ K decreases as $dT/dP \approx -1.0$ K/kbar with increasing pressure.[9] The hcp $\rightarrow \omega \rightarrow$bcc sequence of structural transformations is observed in Zr when investigating the isothermal compressibility at room temperatures. The $\omega \rightarrow$bcc transition has been detected at pressures of 350 ± 50 kbar (Ref. 10) and 330 kbar (Ref. 11).

The authors of the most careful first-principles total energy calculation at $T=0$ for different crystalline modifications of Zr (Ref. 12) in the local density approximation (LDA) have found a high-pressure β phase to arise at 483 kbar. Using the LDA within the framework of density functional theory for the exchange-correlation energy calculation results, as a rule, in an underestimation of the equilibrium volume magnitude. For *d* metals, the generalized gradient approximation[13] (GGA) often considerably improves quantitative agreement of the calculated equilibrium volume with the observed one. We will compare the GGA and LDA approaches in calculating the total energies and the *P-T* phase diagram of Zr by the Debye model. To achieve this aim, we should first construct the Debye model for two hexagonal structures of Zr.

DEBYE MODEL FORMALISM

Let us define the free energy of the system as a sum of the rigid lattice total energy and the free vibrational energy. With neglect of the electron subsystem entropy, we have

$$F(V,T) = E_e(V) + E_D(V,T) - TS_D(V,T). \qquad (1)$$

Here $E_e(V)$ is the total energy of the electron subsystem. In the Debye model, the vibrational lattice energy E_D and the entropy S_D are expressed as

$$E_D(V,T)=3k_BTD(x_D)+E_0, \tag{2}$$

$$S_D(V,T)=4k_B\left[D(x_D)-\tfrac{3}{4}\ln(1-e^{-x_D})\right], \tag{3}$$

where $x_D=\Theta_D/T$, $D(x_D)$ is the Debye function of the heat capacity normalized to unity in the high-temperature limit,[14] and $E_0=\frac{9}{8}k_B\Theta_D$ is the energy of zero-point lattice vibrations.

The final expression for the free energy has the form

$$F(V,T)=E_e(V)-k_BT[D(x_D)-3\ln(1-e^{-x_D})-\tfrac{9}{8}x_D]. \tag{4}$$

Let us describe the technique for calculating Θ_D. Assuming a constant sound velocity, one can write a simple relation between Θ_D and B:

$$\Theta_D=K(aB/M)^{0.5}, \tag{5}$$

where a is the lattice constant in a.u., B is measured in kbar, M in mass a.u., and $K=42.172$. In Ref. 5 it was shown that in cubic nonmagnetic metals a good agreement with the experimental Θ_D can be obtained by the use of Anderson's average for the sound velocity.[4] This makes it possible to choose, for cubic metals, a universal K value of 26.024 which relates quite well the experimental Debye temperature and bulk modulus. However, there is no reason to believe that the same K may be used for noncubic metals as well. The simplest way to define the numerical value of K for noncubic metals is the use of relation (5) with the experimental values of $(\Theta_D)_{\text{expt}}$ and B_{expt}. As a result, the particular K values will differ for both different metals and the crystalline structures of the same metal. Using the obtained value of K and the bulk modulus calculated from the total energy, one can find the theoretical Θ_D and then the free energy (4). Next, the equilibrium volume, bulk modulus, Debye temperature, and Grüneisen constant may be redefined by minimizing $F(V,T)$ for each fixed temperature. Also the temperature dependences of the above quantities and the coefficient of volume expansion are readily calculated (see, e.g., Ref. 5). In our previous paper[8] we showed how the resulting point $T^{\text{hcp}\rightarrow\text{bcc}}$ of the phase diagram depends on the value of K in Ti. A 16% variation of this parameter changes the Debye temperature from 288 to 240 K and decreases the $T^{\alpha\rightarrow\beta}_{P=0}$ by 900 K. Thus the coefficient K may be considered as a free parameter if the experimental data are not available.

For the hexagonal α and ω phases of Zr, the coefficient K in Eq. (4) was taken equal to 32.90, a value determined from the experimental Θ_D (defined by low-temperature specific heat measurements) and B_0 of the equilibrium α phase. The experimental value of B for the high-temperature β-Zr being not available, we used the universal value of $K=26.024$ for cubic structures to calculate Θ_D for both high-temperature and high-pressure β phases.

TOTAL ENERGY CALCULATION

To calculate the band structure, we used the full-potential linear muffin-tin orbital (FP-LMTO) method.[15] When expanding the basis functions in spherical harmonics inside the MT spheres and reexpanding the MT orbitals outside the MT spheres, as well as in expanding the crystalline potential and charge density, the maximum values of the angular momentum l were taken to be 2, 4, and 8, respectively. Three values of the MT orbital tail energy (one for $4p$ states) were chosen to describe the conduction band. In integrating over the irreducible part of the Brillouin zone (BZ), we used 145, 165, and 792 **k** points for β, ω, and α-Zr, respectively. We investigated the convergence of the total energy on increasing the number of **k** points for each structure. So for hcp Zr an increase from 165 to 792 points leads to a total energy difference less than 0.5 mRy. In all the calculation variants, the MT sphere radii were chosen to be equal and corresponding to one of the two types of ω phase atoms: $r_{\text{MT}}=2.747$ a.u. The ratio c/a was taken to be 0.625 for the ω phase and 1.593 for the α phase, which corresponds to the experimental data available. The ratio c/a obtained upon optimization for the ω structure is 0.622 for the equilibrium volume, and the difference in total energy between the ratios 0.625 and 0.622 is less than 0.07 mRy. We did not optimize c/a for the hexagonal phase. As shown in Ref. 10, the ratio c/a for ω-Zr remains unchanged from the beginning of $\alpha\rightarrow\omega$ transformation up to 300 kbar.

The total energy for three phases of Zr was calculated with the GGA (Ref. 13) and LDA for which we used the exchange-correlation potential in the Janak-Williams-Moruzzi (JWM) parametrization.[16] The calculated binding curves were analyzed and the equilibrium properties were defined as in Ref. 5. In interpolating the binding curves we used 8 (for the hexagonal structures) and 17 (for the bcc one) calculated energy–vs–reduced-volume points. The binding curves for three known structures of Zr are presented in Fig. 1. Our total-energy calculations of equilibrium lattice properties at $T=0$ for α-Zr are illustrated in Table I. In discussing the GGA effect, it should be noted that, first, the theoretical equilibrium volume exceeds the experimental one by only 0.3% and, second, the GGA binding curve shape improves the value of the bulk modulus. In Ref. 18 the bulk modulus for α-Zr was calculated through a combination of elastic constants, and its value $B_0=1.03$ Mbar agrees well with our GGA result. For the ω phase, the GGA calculation gives $B_0=1.13$ Mbar at the total-energy minimum, while the experimental value for this phase is equal to 1.21 Mbar.[11] The experimental estimate of the bulk modulus for the β phase is 2.03 Mbar,[11] whereas our calculation yields 2.18 Mbar at $V/V_0=0.7$.

An analysis of the total-energy curves that intersect with decreasing volume shows that both our models reproduce the $\alpha\rightarrow\omega\rightarrow\beta$ sequence of structural transformations in Zr. The data listed in Table I allow one to perform the quantitative analysis. For the $\omega\rightarrow\beta$ transition, the volume and the volume change are in reasonable agreement with the experiment, while in the case of the $\alpha\rightarrow\omega$ transition we have obtained a somewhat overestimated volume value with respect to the observed one. The degree of the deviation from the experimental data for different exchange-correlation potentials is determined by the shift of binding curves towards larger volumes and the intrinsic shape of these curves. The experimental $\omega\rightarrow\beta$ interface has a negative slope of

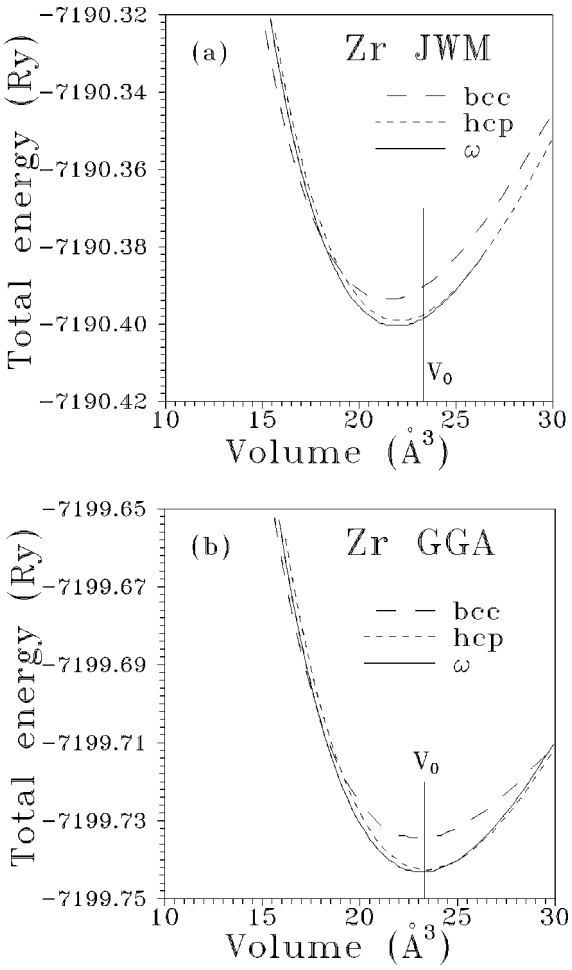

FIG. 1. The total energy vs the volume for three phases of Zr for the LDA (a) and GGA (b). The solid vertical line corresponds to the experimental volume for α-Zr.

-3.9 ± 0.5 K/kbar at room temperatures,[10] whereas the $\alpha \rightarrow \omega$ interface has, on the contrary, a positive $dT/dP=16$ K/kbar.[9] In extrapolating the experimental data to lower temperatures, better agreement with our interfaces calculated at $T=0$ may be obtained. But we did not perform extrapolation as we believe that for lower temperatures the experimental slope value will be different. Besides, for the low-temperature region $T<\Theta_D/4$ we have to account for the

TABLE I. The equilibrium volume V_0 (in Å^3), the bulk modulus B_0 (in Mbar), and the reduced volumes of the structural transformations of α-Zr calculated within the GGA and LDA schemes at $T=0$, as compared to the experimental data and the data obtained within the Hedin-Lundqvist LDA scheme.

	V_0	B_0	$V_{\alpha\rightarrow\omega}$	$V_{\omega\rightarrow\beta}$	$\Delta V_{\omega\rightarrow\beta}/V$
Expt. [a]	23.3	0.83	0.997	0.764	1.6 %
LDA (H-L) [b]	22.5	1.19			
LDA (H-L) [c]	22.2			0.69	
LDA (JWM)	22.07	1.11		0.77	2.2 %
GGA	23.37	1.03		0.764	2.5 %

[a]Reference 9.
[b]Reference 17.
[c]Reference 12.

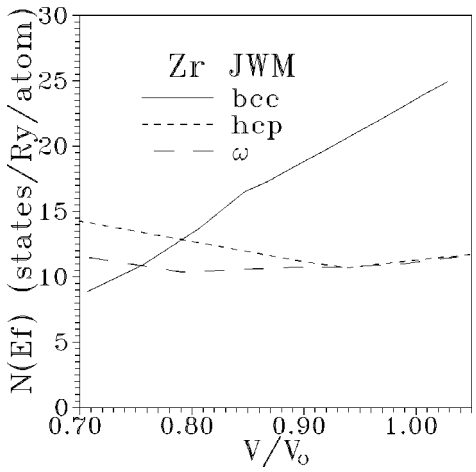

FIG. 2. The density of states at the Fermi level vs the reduced volume for different structures of Zr within the LDA.

entropy term of the electron subsystem and electron-phonon interaction.

In accordance with our calculations, the ground state of Zr corresponds to the ω structure. The LDA total-energy difference between the minima of ω and α phases amounts to 1.43 mRy, whereas the GGA one is 0.8 mRy. Note that in Ref. 12 the total-energy minimum for Zr corresponds to the ω phase as well. Thus, according to the latest *ab initio* calculations, the open ω phase, being not intrinsic for the *d* metals, is realized at high pressures in group-IVa elements and moreover it exhibits the minimum energy. Presumably, model improvements such as the full potential involvement, the relativistic generalization, or the exchange-correlation potential variation will not change the energetic competition between the α and ω phases. In practice we always carry out investigations at finite temperatures. Therefore the density functional theory is not always apt to reproduce the real situation. Adding the electron entropy term will probably result in a change of the free energy difference between α- and ω-Zr. Such consideration, though being very interesting, is beyond the scope of this work.

The competitive behavior of the α and ω phases in the ambient pressure region can be seen in Fig. 2, where the density of states at the Fermi level, $N(E_F)$, is plotted versus the reduced volume V/V_0 for all the structures of Zr. To $V/V_0=0.94$ ($P\sim60$ kbar), the density of states at E_F is actually the same for the α and ω phases. In the range $0.76<V/V_0<0.94$, the ω structure has the lowest $N(E_F)$, and for $V/V_0<0.76$ ($P>450$ kbar) the β phase becomes preferential. The GGA model brings about insignificant changes in Fig. 2.

Figure 3(a) displays the dependence of the occupied part of the conduction band at the Γ point of the BZ, E_F-E_{5s}, on the compression. As expected, the width of the conduction band and its occupied part increase as the reduced volume decreases. But at $V/V_0<0.77$, and only for the ω and β phases, the occupied part of the conduction band begins to diminish, becoming quantitatively close for both structures. One can suppose that this effect is due to the $4p$ states which approach the conduction band bottom from below. It might be useful to illustrate the behavior of upper core states under the lattice compression.

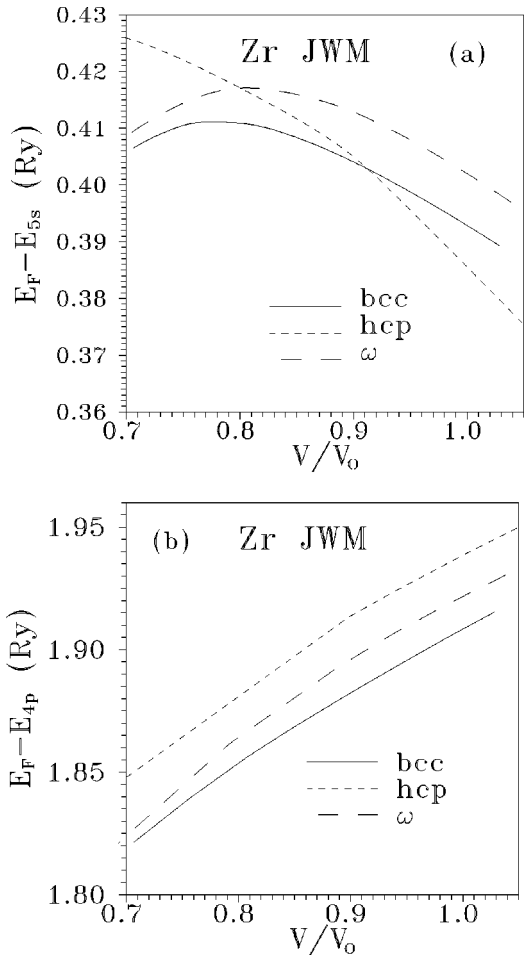

FIG. 3. The occupied part of the conduction band E_F-E_{5s} (a) and the energetical position of the $4p$ states with respect to the Fermi level E_F-E_{4p} (b) in Zr against the reduced volume within the LDA.

In Fig. 3(b), the difference between E_F and the energy of the $4p$ state at the Γ point of the BZ is shown as a function of the reduced volume. The difference E_F-E_{4p} changes only slightly in passing from the LDA to the GGA, and so we restrict ourselves to the LDA case illustration. When the specific volume is reduced by 30%, which corresponds to the region of existence of β-Zr, the position of $4p$ states approaches E_F, as well as the conduction band bottom, by $\sim$0.1 Ry. Note that the considered energy difference E_F-E_{4p} becomes, at high pressures, actually the same for the ω and β phases. The width of the $4p$ band, which is found to be 65 mRy at the Γ point of ω-Zr for V_0, reaches at $V/V_0=0.7$ the value of 179 mRy (or 225 mRy from the density of states calculation). To date the isothermal compressibility of Zr at room temperature has been studied in the pressure range up to 680 kbar. The experimental data obtained in Ref. 11 at 560 kbar have been associated by the authors with an isostructural β-Zr transition. We have found no peculiarities in the total energy of β-Zr in the high-pressure region.

In Ref. 12 the electron density distribution patterns are presented for the selected cell sections of all Zr structures. The main distinction of the ω phase from the others is the pronounced covalent character of the chemical bond. This result is confirmed by our GGA calculation. The decisive role in the behavior of the electron density outside the MT

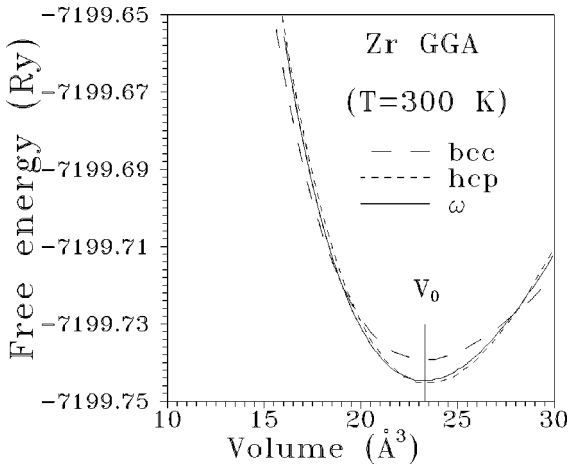

FIG. 4. The free energy vs the volume for three phases of Zr within the GGA. The solid vertical line corresponds to the experimental volume for α-Zr.

spheres is played by the p states of the conduction band. In our opinion, a specific distribution of the electron density may be responsible for the appearance of a local minimum of the total energy under distortion of the perfect ω structure. The experimental data[19] are indicative of the metastable ω phase retention after loading zirconium with converging

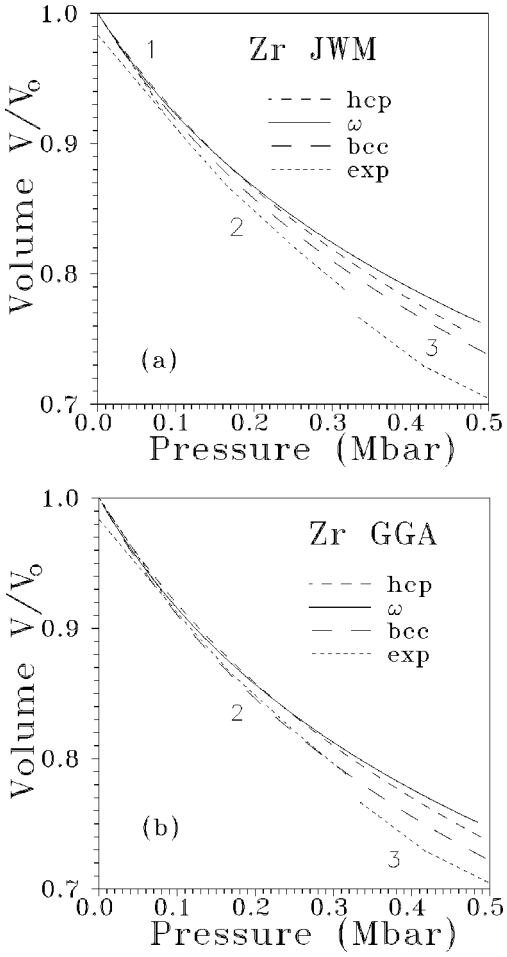

FIG. 5. The calculated dependences $P(V)$ of Zr at $T=300$ for the LDA (a) and GGA (b). Experimental data from Ref. 11: 1, α; 2, ω; and 3, β phases.

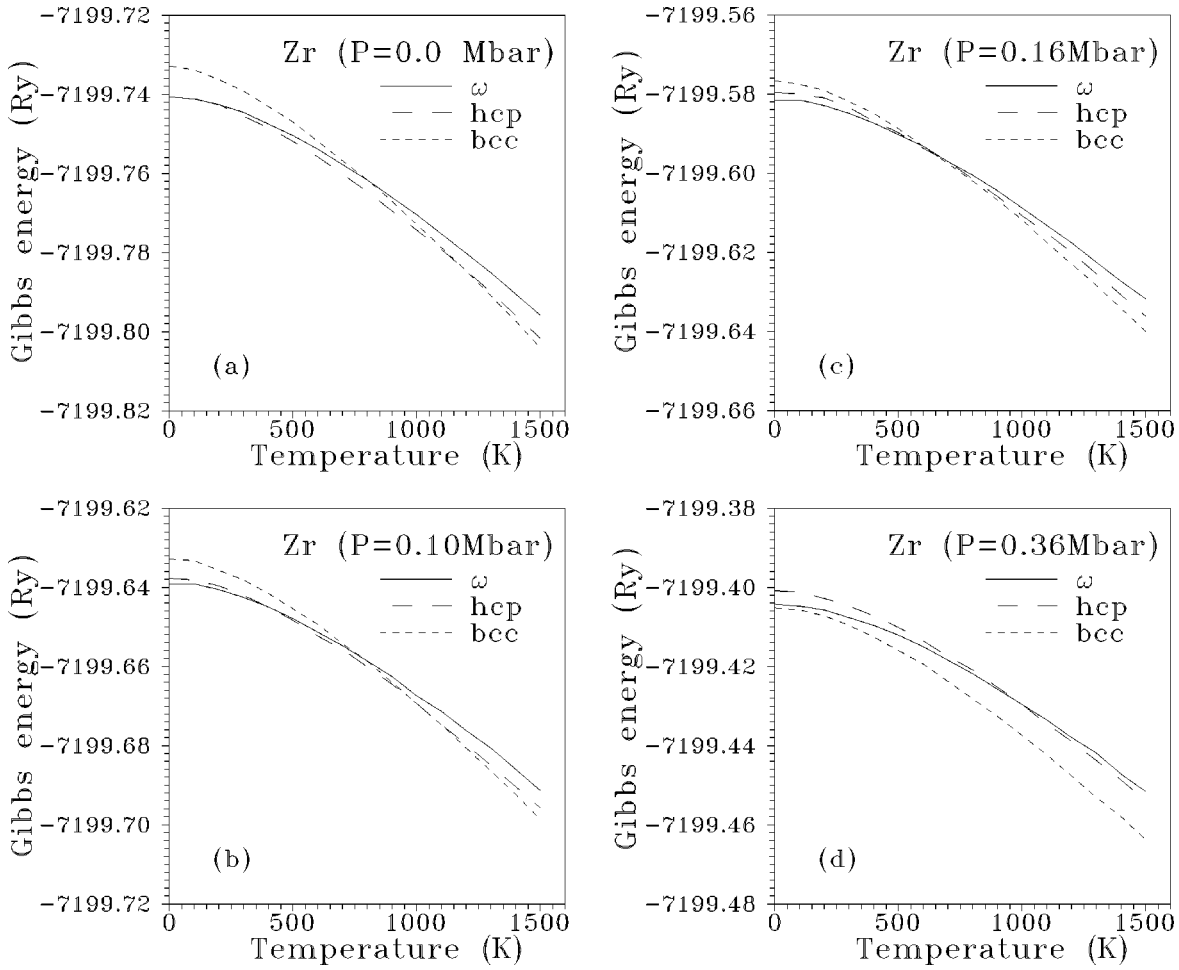

FIG. 6. The temperature dependences of the Gibbs energy for different pressures: $P=0$ (a), $P=0.1$ Mbar (b), $P=0.16$ Mbar (c), and $P=0.36$ Mbar (d).

shock waves. In a recent work,[20] Raman scattering was used to study the pressure dependence of lattice modes in Zr to 160 kbar. An additional mode, observed above 80 kbar in the unloading cycle, is assigned to ω-Zr. This fact can be interpreted in favor of the existence of a metastable ω phase.

P-T PHASE DIAGRAM

Consider now the improvements brought about by the use of the Debye model in studying the structural stability of Zr. Figure 4 plots the free energy versus the specific volume for three structures of Zr within the GGA. The α phase has the lowest $F(V,T)$ at room temperature, and this ensures qualitative agreement of the calculated phase diagram with the experimental one. The Debye temperature and the Grüneisen constant we calculated for the theoretical equilibrium volume of α-Zr at $T=300$ K within the GGA were 285.7 K and 0.67, whereas the LDA values were found to be 279.1 K and 1.02, respectively. For comparison, the corresponding experimental values are 291 K and 0.77.[22]

To construct the phase diagram, the thermodynamical Gibbs potentials $G(P,T)$ should be calculated and compared for three structures on a fixed mesh of independent parameters (P,T):

$$G(P,T)=F(V,T)+PV. \tag{6}$$

The isothermal dependences $P(V)$ were calculated by direct differentiation of free energy $P=-(\partial F/\partial V)_T$ for each structure.

The $P(V)$ curves obtained at $T=300$ K within the GGA and LDA approaches are shown in Fig. 5. The experimental curves in these figures are taken from Ref. 11 in which they were constructed by the method of least squares in such a manner as to satisfy the Birch-Marnaghan equation[21] by fitting the parameters B_0 and B_0' for each phase. On the basis of theoretical curves for the equation of state, the specific volume was found at fixed values of temperature and pressure and then used in calculating the Gibbs energies (6).

The procedure for defining the points of interfaces is illustrated by Fig. 6 displaying the temperature dependences of the Gibbs energy for $P=0$, $P=0.1$ Mbar, $P=0.16$ Mbar, and $P=0.36$ Mbar. At $P=0$, in the range $0<T<1193$ K, the Gibbs potential is minimum for the α phase; further, at $T>1193$ K the β phase is realized. The points of intersection of the curves in Fig. 6 determine the interfaces of the P-T diagram. Figure 6 for $P=0.16$ Mbar corresponds to the triple point of the phase diagram. The figure for $P=0.36$ Mbar demonstrates the formation of a high-pressure β phase.

The calculated P-T phase diagram is presented in Fig. 7. The theoretical temperature of the $\alpha\rightarrow\beta$ transition at zero

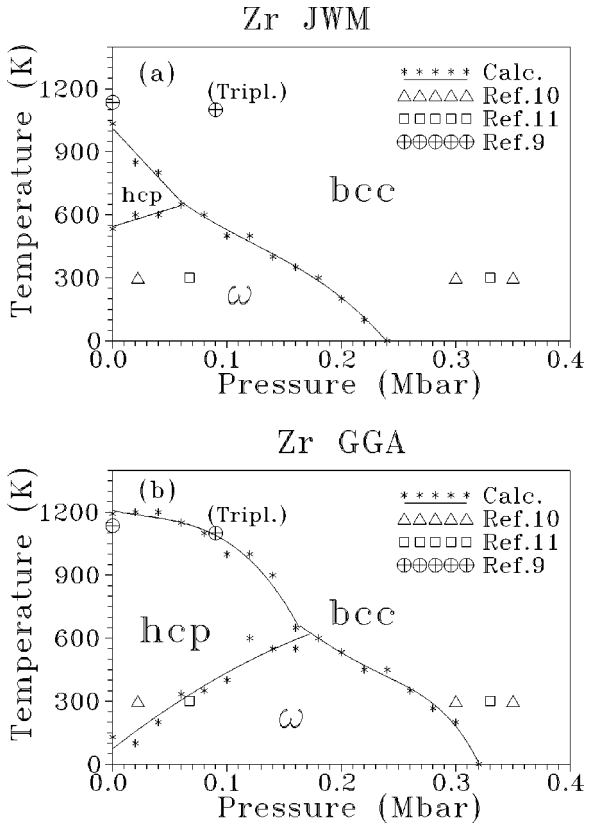

FIG. 7. The P-T diagram of Zr for the LDA (a) and GGA (b).

pressure within the GGA differs from the experimental value by only 60 K. The magnitude of K for all structures in this work was assumed to be temperature and pressure independent. The characteristic points of the P-T phase diagram are listed in Table II. Within the GGA the diagram reproduces quite well the available experimental data on the temperature- and pressure-induced structural transformations in Zr. The triple point estimated from the experiments, though being distant in temperature from that obtained by us, nevertheless belongs to the calculated $\alpha \rightarrow \beta$ interface.

TABLE II. The basic points of the P-T diagram of Zr (P in kbar, T in K).

	$T^{\alpha\rightarrow\beta}_{P=0}$	$P^{\alpha\rightarrow\omega}_{T=300}$	$P^{\omega\rightarrow\beta}_{T=300}$	P_{triple}	T_{triple}
Expt.	1136	33-67	350±50	~90	~1100
LDA	1034		180	60	650
GGA	1193	54	270	160	620

CONCLUSION

In this work we tried to demonstrate, first, the possibility of calculating the P-T phase diagram of Zr within the framework of a rather simple Debye model and, second, the dependence of the calculation results on the choice of the exchange-correlation potential. Quantitative agreement with experiments was obtained only when using the GGA, which scheme does not seem to be universal for all metallic systems. Zirconium, however, proved to be an appropriate subject of investigation by the GGA. We expect that the suggested model may be successfully applied in calculating the phase diagrams of more complex systems as well.

ACKNOWLEDGMENTS

The authors are indebted to S. Savrasov for the FP-LMTO code and to E. Salamatov, E. Chulkin, and G. Sin'ko for helpful discussions. We want to thank H. Olijnyk and A. P. Jephcoat for providing us with their paper before publication.

[1] F. Ducastelle, in *Order and Phase Stability in Alloys, Cohesion and Structure*, edited by F. de Boer and D. Pettifor (North-Holland, Amsterdam, 1991), Vol. 3.
[2] A. Mookerjee, N.-X. Chen, V. Kumar, and M. A. Satter, J. Phys.: Condens. Matter **4**, 2439 (1992).
[3] G. Davidov, D. Fuks, and S. Dorfman, Phys. Rev. B **51**, 13 059 (1995).
[4] O. L. Anderson, in *Physical Acoustics*, edited by W. P. Mason (Academic, New York, 1965), Vol. III-B, p. 43.
[5] V. L. Moruzzi, J. F. Janak, and K. Schwarz, Phys. Rev. B **37**, 790 (1988).
[6] S. A. Ostanin, E. I. Salamatov, and V. Yu. Trubitsin (unpublished).
[7] E. I. Salamatov, Phys. Status Solidi B **197**, 323 (1996).
[8] S. A. Ostanin and V. Yu. Trubitsin, J. Phys.: Condens. Matter **9**, L491 (1997).
[9] Yu. Tonkov, *Phase Diagram of the Elements Under Pressure* (Nauka, Moscow, 1979).
[10] H. Xia, S. J. Duclos, A. L. Ruoff, and Y. K. Vohra, Phys. Rev. Lett. **64**, 204 (1990); H. Xia, A. L. Ruoff, and Y. K. Vohra, Phys. Rev. B **44**, 10 374 (1991).
[11] Y. Akahama, M. Kobayashi, and H. Kawamura, J. Phys. Soc. Jpn. **60**, 3211 (1991).
[12] R. Ahuja, J. Wills, B. Johansson, and O. Eriksson, Phys. Rev. B **48**, 16 269 (1993).
[13] J. P. Perdew and Y. Wang, Phys. Rev. B **45**, 13 244 (1992); M. Levy and J. Perdew, *ibid.* **48**, 11 638 (1993).
[14] L. A. Girifalco, *Statistical Physics of Materials* (Wiley, New York, 1973).
[15] S. Yu. Savrasov and D. Yu. Savsasov, Phys. Rev. B **46**, 12 181 (1992).
[16] V. L. Moruzzi, J. F. Janak, and A. R. Williams, *Calculated Electronic Properties of Metals* (Pergamon, New York, 1978).
[17] M. M. Sigalas and D. A. Papaconstantopoulos, Phys. Rev. B **50**, 7255 (1994).
[18] L. Fast, J. M. Wills, B. Johansson, and O. Eriksson, Phys. Rev. B **51**, 17 431 (1995).
[19] E. A. Kozlov, B. V. Litvinov, E. A. Abakshin, A. V. Dobromyslov, N. I. Taluts, N. V. Kazantseva, and G. G. Taluts, Fiz. Met. Metalloved. **79**, 113 (1995).
[20] H. Olijnyk and A. P. Jephcoat (unpublished).
[21] F. Birch, J. Geophys. Res. **83**, 1257 (1978).
[22] *Handbook: Physical Values*, edited by I. S. Grigoryev and E. Z. Meilihov (Energoatomizdat, Moscow, 1991).